

Metallically gradated silicon nanowire and palladium nanoparticle composites as robust hydrogenation catalysts

Yoichi M. A. Yamada ^{1✉}, Heeyoel Baek¹, Takuma Sato¹, Aiko Nakao² & Yasuhiro Uozumi ³

Heterogeneous catalysis of alkenes to alkanes is of great importance in chemical industry, but more efficient and reusable heterogeneous catalysts are still demanded. Here, we report a metallicly gradated composite of a silicon nanowire array and palladium nanoparticles which are reused for the hydrogenation of an alkene. The catalyst promotes the hydrogenation of stilbene with atmospheric hydrogen (0.1 MPa) to give diphenylethane quantitatively. The recovered catalyst can be reused, and mediates the reaction without loss of yield more than one hundred times, whereas the stability of Pd/C degrades rapidly over 10 cycles of reuse. The catalyst allows the hydrogenation of a variety of alkenes, including tetra-substituted olefins. Structural investigation reveals that palladium nanoparticles are metallicly gradated onto the silicon nanowire array under mild conditions by agglomeration of palladium silicide, as confirmed by XAFS and XPS together with argon-ion sputtering. This means of metal agglomeration immobilization may be applicable to the preparation of a variety of metal nanoparticle catalysts.

¹RIKEN Center for Sustainable Resource Science, Wako, Saitama 351-0198, Japan. ²Bioengineering Laboratory, RIKEN, Wako, Saitama 351-0198, Japan. ³Institute for Molecular Science (IMS), Okazaki, Aichi 444-8787, Japan. ✉email: [ymayamada@riken.jp](mailto:yamayada@riken.jp)

If catalysts worked perpetually with high catalytic activity, the chemical industry and catalytic science would benefit. Toward achieving this ultimate goal of catalytic science, researchers have developed highly active and reusable heterogeneous catalysts. Hydrogenation is a very important reaction in chemical processes, and thus, the development of highly reusable catalysts for hydrogenation is highly important and challenging^{1–4}. Heterogeneous catalysts have been prepared mainly in two ways: the first is the immobilization of the metal species on solid supports through surface adsorption. Pd/C and Pd on metal oxides (SiO₂, Al₂O₃, MgO, CeO₂, etc.) are typical examples of this type (Fig. 1a)^{5–14}. The other is the immobilization of metal species in solid matrices of polymers, dendrimers, and organic frameworks via coordinative interactions, where the metal species are stabilized through the steric bulk of the frameworks and/or the coordinative interactions with heteroatoms (e.g. N, O, P, and S) (Fig. 1b)^{15–25}. For example, we have developed convoluted polymeric metal catalysts that promote various cross-couplings and Huisgen cycloadditions at mol ppm level loadings^{26–31}. However, the adsorption and coordination interactions in these catalysts are generally weaker than those resulting from covalent and metal bonds, and may thus cause metal leaching problems, particularly in industrial applications.

To address these challenges, we envisioned the immobilization of metal nanoparticles on supports via bonding with the alloy/agglomeration of the metal nanoparticles and supports. In such an approach, the metal nanoparticles would be strongly anchored to the support via metallic bonds (Fig. 1c), and should overcome the traditional issues and improve catalysis.

The surface structure of support materials is known to significantly affect the catalytic activity and selectivity of a transformation. Nanostructured materials are attractive candidates as supports for transition metal nanoparticles for preparation of catalysts for sustainable and efficient chemical processes³². We have been interested in nanoscale reactions on support materials for the development of catalytic reactions for efficient organic transformations. Recently, we reported the development of a silicon nanowire array and palladium nanoparticle hybrid (SiNA-Pd) for catalytic organic transformations^{33,34}. Here we investigate the reusability of this system for the hydrogenation of olefins, where the catalyst can be readily reused more than one hundred times without loss of catalytic activity. In contrast, the catalytic activity of Pd/C for the same transformation decreases during its reuse, and afforded

much lower catalytic activity. Further investigation revealed that the palladium nanoparticles (PdNPs) were anchored to the silicon as palladium silicides via Pd–Si metallic bonds, and gradually form an agglomerated Pd/Si alloy layer as shown in Fig. 1c.

In this communication, we present the high reusability and catalytic activity of SiNA-Pd for the hydrogenation of olefins, including tetra-substituted alkenes. We also show evidence of the immobilization mode of the metal nanoparticles on the supports through gradated alloy formation/agglomeration of the metal nanoparticles and the supports.

Results and discussion

High reusability for hydrogenation. SiNA-Pd was reproducibly prepared in accordance with our previous report (Fig. 2), where palladium nanoparticles were installed into SiNA by reduction of Pd(II) on the SiNA surface carrying terminal hydrogens (see Supplementary method for details)^{35–41}. The hydrogenation of *trans*-stilbene (**1a**) was carried out with SiNA-Pd corresponding to 0.12 mol% of Pd under 0.1 MPa hydrogen gas conditions and afforded bibenzyl (**2a**) in quantitative yield. The recovered catalyst was reused without loss of catalytic activity 150 times more in the same reaction and afforded **2a** quantitatively in all conversions (Fig. 3). Notably, the turnover number of the catalyst in the consecutive reactions reached 125000. No Pd was detected in the reaction mixture using ICP-MS analysis (detection limit: 0.021 ppb), which indicated the lack of Pd leaching during the catalytic transformation. In contrast, the catalytic activity of Pd/C decreased significantly during its consecutive reuse, which is in-line with the literature reports^{42,43}.

Hydrogenation of various alkenes. With a highly reusable catalyst in hand, the hydrogenation of various alkenes was evaluated with 500 mol ppm (0.05 mol%) Pd of SiNA-Pd (1/SiNA-Pd = 2000/1 (mol/mol)) (Fig. 4). In all of the reactions presented in Fig. 4, the catalyst was reused to show the generality of its reusability. When the reaction of the less reactive tetra-substituted alkenes **1b–c** was carried out (Supplementary Data 1), we were pleased to find that the reaction proceeded smoothly to give the corresponding alkane **2b–c** in >99% and 96% yields, respectively. The recovered catalyst promoted the reaction to give **2b** in >99% and 97% yields (2nd use of SiNA-Pd), and in >99% and 96% yields (3rd use of SiNA-Pd), respectively (Entries 1 and 2) (Supplementary Data 2). Tri- and di-substituted alkenes, including aliphatic olefins, as well as an alkyne and an imine (**1b–k**) were readily converted by the fresh and recovered SiNA-Pd under similar conditions to the corresponding products **2b–i** in 91–99% yields (Entries 3–10).

SiNA-Pd was applied to the hydrogenation of fatty acids and triolein under neat conditions (Fig. 5). Full conversion of unsaturated fatty acids to saturated fatty acids is important for preventing the formation of *trans*-fatty acids^{44–49}. The hydrogenation of oleic acid (**1l**) was performed and gave stearic acid (**2j**), a fatty acid which activates high density lipoprotein (HDL) and decreases low density lipoprotein (LDL)⁵⁰, in >99% yield (Fig. 5a). SiNA-Pd was reused under similar conditions and gave **2j** in >99% yield. Linoleic acid (**1m**) was also converted to **2j** in >99% yield (Fig. 5b). Triolein (**1n**) also underwent hydrogenation to give glyceryl tristearate (**2k**) in 99% yield (Fig. 5c).

In SiNA-Pd, the palladium nanoparticles are immobilized by the reduction with the silanes on the silicon surface. We hypothesized that the palladium nanoparticles were metallicly gradated onto the silicon nanowire array via strong metal bonding (alloy/agglomeration) between the palladium and silicon. Although we attempted studying the metal bonding in SiNA-Pd to gain insight into the immobilization mode of the

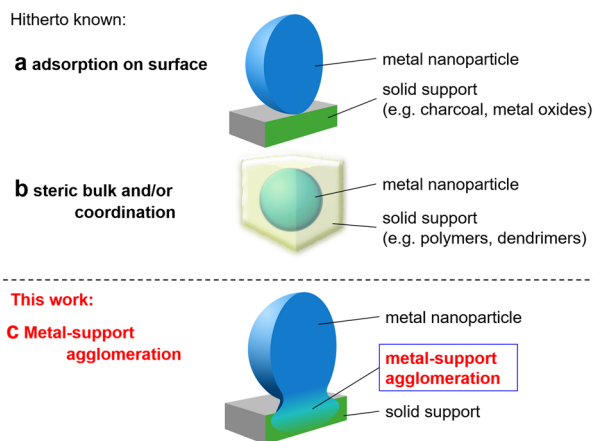


Fig. 1 Morphology of metal-support stabilization in solid-supported metal nanoparticle catalysts. **a** Surface adsorption. **b** Steric bulk and/or coordination. **c** Gradient agglomeration of metal nanoparticle and support material (this work).

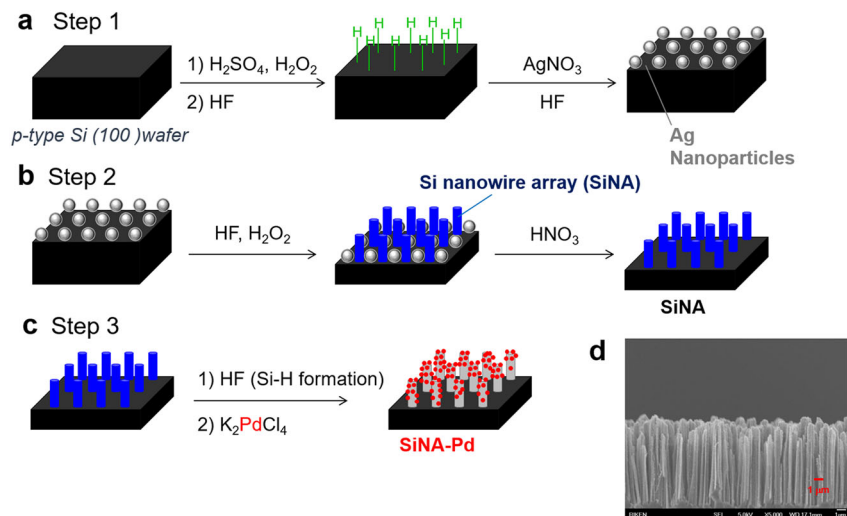


Fig. 2 Schematic illustration for preparation of SiNA-Pd. **a** Hydrogen-termination of Si(100) surface, followed by deposition of silver nanoparticles. **b** Formation of SiNA by metal-assisted chemical etching. **c** Preparation of SiNA-Pd through reductive deposition of palladium species. **d** SEM image of SiNA-Pd.

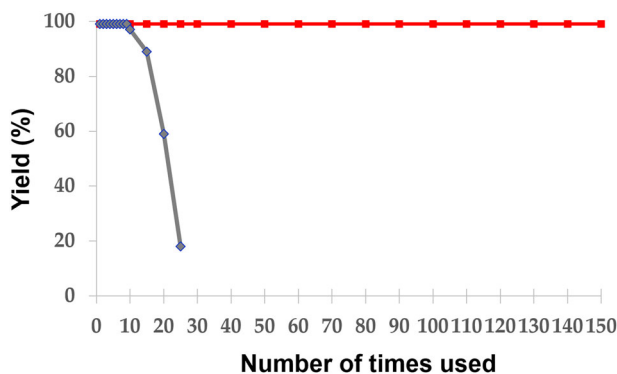


Fig. 3 Hydrogenation of trans-stilbene (1a) for comparison with catalytic activity of SiNA-Pd and Pd/C. trans-stilbene (1a) (0.5mmol), catalyst (0.12mol%), ethanol (2.0mL) under H_2 (0.1MPa) at 70°C for 24h. Red: SiNA-Pd; blue: Pd/C.

metal nanoparticles on supports, the spectroscopic analysis was not feasible due to the high steric crowding of SiNA-Pd with palladium nanoparticles and silicon nanowires. To address this limitation, we prepared less crowded silicon-nanostructured palladium nanoparticles under similar conditions for the following investigation.

Elucidation of stable Pd-Si nanoparticle formation in the catalyst. X-ray photoelectron spectroscopy (XPS) allows relatively high surface-sensitive spectroscopic analysis, because the mean free path of photoelectrons in solid materials is within several nanometers from the outermost surface, and the technique is often utilized in combination with sputtering techniques for the purpose of depth analysis⁵¹. Remarkably, a series of XPS spectra of the silicon-nanostructured palladium nanoparticles for Pd 3d core level exhibited the presence of palladium silicide⁵² besides Pd(0) (Fig. 6). Ar-ion-sputtering was performed with 3-keV kinetic energy in vacuum. The XPS spectra were recorded at a take-off angle of 90°. The as-prepared silicon-nanostructured palladium nanoparticles were etched by sputtering for up to 16 min in vacuum, and the nominal etching rate was determined to be 0.5 nm/min of SiO_2

using a SiO_2/Si standard. With the increase in the sputtering time, the peak intensity of Pd(0) (ca. 335 eV for Pd $3d_{5/2}$) decreased, whereas the intensity in the higher binding energy region (similarly 336–338 eV) increased. The surface oxides on PdNPs (usually described as Pd(II)O and Pd(IV)O₂ (It is known that palladium dioxide synthesized at a high oxygen pressure decomposes at temperatures above 340 K)^{53,54}) should be removed from the surface of the sample after the etching. Indeed, a weak and very broad peak with a significantly high binding energy (>338 eV for Pd $3d_{5/2}$) almost completely disappeared after a sputtering time of 1 min, which is attributed to the surface PdO₂ localized within the block boundaries of PdO⁵⁵. We suppose that the reason for the increased intensity in the high binding energy region in the 335–338 eV range for Pd $3d_{5/2}$ is due to the depth distribution of the palladium species. Thus, the higher binding energy species localize behind the Pd(0) nanoparticles. Furthermore, the binding energy of the main peak near 336 eV in the spectra of the etched samples was not consistent with that of PdO in the surface-oxidized palladium foil (336.9 eV)⁵⁵. Over a period of the sputtering, the intensity of the broad peak derived from SiO_2 near 102.6 eV in the spectra for Si 2p core level decreased monotonically relative to that of bulk silicon, which indicates the etching of the SiO_2 surface along with that of the palladium oxide and bulk palladium. In addition, the peak shape of the crystalline silicon (split into $2p_{1/2}$ and $2p_{3/2}$ due to spin-orbit coupling) in the 98–100 eV range was continuously deformed during the etching. As is the case with a series of Pd 3d spectra, this indicated that the contribution of palladium silicide increased in the early stage of the etching, which affected the peak shape around 99 eV in the Si 2p spectra due to the removal of Pd(0).

We were successful in separating the peak components of Pd (0), and palladium silicide (Pd₄Si, Pd₃Si, Pd₂Si, and PdSi) in the Pd 3d spectrum at a sputtering time of 4 min (Fig. 7). The envelope was fitted at 334.6/339.8 eV ($3d_{5/2}/3d_{3/2}$) for Pd(0), 335.4/340.6 eV for Pd₄Si, 336.1/341.3 eV for Pd₃Si, 336.9/342.1 eV for Pd₂Si, and 337.8/343.08 eV for PdSi. The values of full width at half maximum (FWHM) were within the range of 0.9–1.3 eV, and these values of binding energy and FWHM were consistent with those reported in earlier research⁵⁵. According to the observations in Fig. 6, in which the population of Pd $3d_{5/2}$ peaks gradually shifted toward the higher binding energy region with an

Entry	Substrate	Product	Yield (%) (1st use of SiNA-Pd)	Yield (%) (2nd use of SiNA-Pd)
1 ^[b]			>99	>99 (>99) ^[c]
2 ^[b]			96	97 (96) ^[c]
3			99	98
4			98	96
5			99	99
6			99	99
7			96	91 (97) ^[c]
8			97	97 (97) ^[c]
9			91	91
10			>99	>99

Fig. 4 Hydrogenation of alkenes by using fresh and used SiNA-Pd under hydrogen atmosphere (0.1 MPa). **a** Conditions: 1 (0.5 mmol), H₂ (0.1 MPa), SiNA-Pd (500 mol ppm Pd), EtOH (2 mL), 70 °C, 12 h. **b** The reaction time: 24 h. **c** Yield in the 3rd use of SiNA-Pd.

increase in the etching time, the more silicon-rich silicide was distributed far from the outermost surface than the palladium-rich silicide and Pd(0). We also performed curve fitting on the Si 2p spectrum at the sputtering for 4 min to separate the peak components of crystalline silicon ($2p_{1/2}$ and $2p_{3/2}$), palladium silicide, SiO_x (suboxide), and SiO₂. The envelope was fitted at 98.4 eV for $2p_{3/2}$, 99.2 eV for $2p_{1/2}$, 99.3 eV for Pd_xSi, 101.0 eV for SiO_x, and 102.6 eV for SiO₂. The values of FWHM are 0.7, 0.7, 2.3, 1.7, and 1.7 eV, respectively. Due to the very close chemical shifts of palladium silicide^{56–58}, we let a somewhat broad peak (FWHM is 2.3) represent the sum of palladium silicides. The peak deformation near the crystalline silicon during the etching is possibly attributed to the increasing contribution of the palladium silicide due to the removal of Pd(0) from the surface toward the silicide phase.

We evaluated the chemical state of the palladium in silicon-nanostructured palladium nanoparticles by Pd L₃-edge X-ray absorption near-edge structure (XANES), which is often used to probe the unfilled *d* orbitals of transition metals (Fig. 8)^{59–61}. (The surface of Pd foil was cleaned by Ar-ion-sputtering prior to the measurement to remove the surface oxide layer of palladium. The samples were transported for analysis at BL-13 beamline of Ritsumeikan SR Center (Shiga, Japan) without air-exposure.) The curve fitting for the near-edge region in the spectrum of silicon-nanostructured palladium nanoparticles was also performed to distinguish the chemical species in the higher-energy region to Pd (0) in the Pd L₃-edge spectrum. Two pseudo-Voigt functions and one error function were applied to the two peaks (one of them is Pd (0)) and baseline (edge-jump of Pd L₃-edge), respectively. The best fit with two peaks ($E_0 = 3174.2$ and 3177.6 eV, where E_0 is the

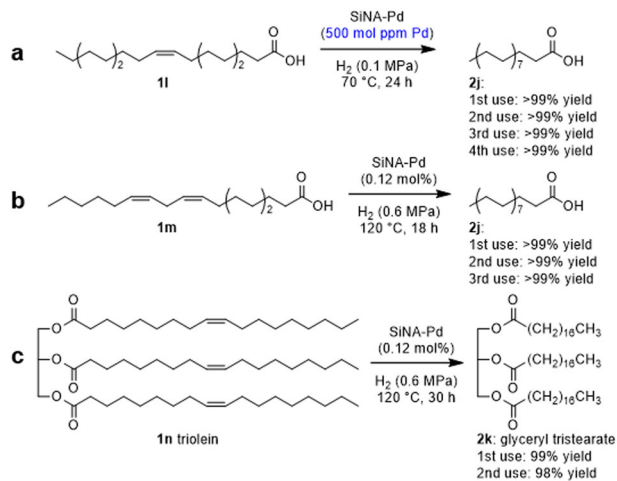


Fig. 5 Hydrogenation of fatty acids. **a** Oleic acid (0.5 mmol), SiNA-Pd (500 mol ppm), H_2 (0.1 MPa), 70 °C, 24 h. **b** Linoleic acid (0.5 mmol), SiNA-Pd (0.12 mol%), H_2 (0.6 MPa), 120 °C, 18 h. **c** Triolein (0.5 mmol), H_2 (0.6 MPa), 120 °C, 30 h.

centroid energy of line) showed good agreement (R-factor: 0.4%) with the experimental line shape of the silicon-nanostructured palladium nanoparticles in the range 3165–3180 eV. The E_0 value of 3174.2 eV (fixed during fitting) is identical to that obtained from the fitting result for the spectrum of Pd foil. As expected, another peak (optimized for all parameters) appeared at a significantly higher E_0 (3177.6 eV) and was slightly broader compared with Pd(0); this peak was assigned to the sum of palladium silicides. Additionally, the IR experiments indicated that after the formation of palladium nanoparticles on the HF-treated silicon surface, the surface Si–H were completely consumed and an oxidized surface of silicon was generated (Supplementary Fig. 1).

Taking all these observations into account, we proposed an immobilization mechanism for the reduction of Pd(II) species onto the silicon surface comprising terminal hydrogens (Fig. 9). The initial step in the formation of PdNPs is the generation of palladium silicides, which are formed in the reaction of Pd(II) with the surface Si–H_x. Subsequently, more palladium-rich silicide species (Pd₂Si, Pd₃Si, and Pd₄Si) are also generated, and the PdNPs grow on the silicides associated with the reduction of Pd(II) by the surface Si–H and Si–Si bonds. The latter pathway (reduction of Pd(II) by the cleavage of Si–Si bond) can explain the reason for the mismatch between the amounts of surface hydrides and PdNPs. Thus, Pd(II) species are reduced by not only the surface Si–H but also Si–Si bonds near the surface. The silicon substrate serves as a reducing agent and the electrons are provided through the palladium silicide layer to the outermost surface of PdNPs at which the reduction of Pd(II) to Pd(0) occurs. Overall, the immobilization of palladium onto silicon is so robust and stable that the catalyst is reusable more than one hundred times without loss of catalytic activity.

We found that our silicon nanowire array-stabilized palladium nanoparticle catalyst (SiNA-Pd) can be reused more than one hundred times without loss of catalytic activity in alkene hydrogenation, and affords the corresponding alkanes quantitatively. A variety of alkenes including tetra-substituted olefins were readily converted to alkanes in high yield by fresh and reused SiNA-Pd. Metallically graded Pd–Si nanoparticles formed on SiNA-Pd provided perpetual heterogeneous catalysis of hydrogenation. Since this methodology for immobilizing metal nanoparticles onto silicon nanowire arrays is promising, we are developing other metal catalysts for organic transformations by utilizing our methodology.

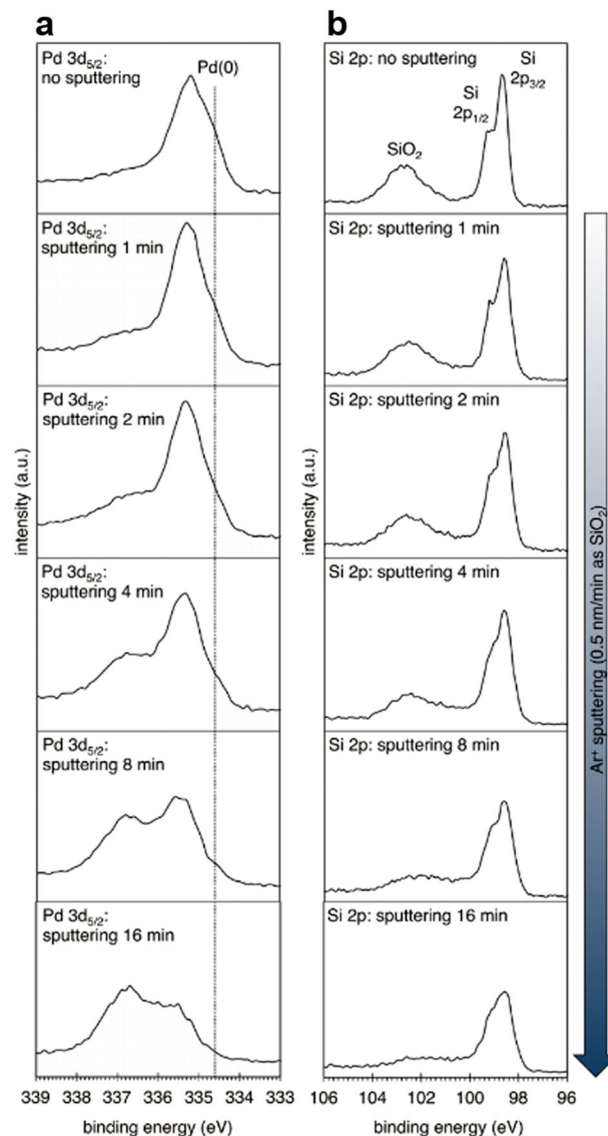


Fig. 6 Study of Pd 3d_{5/2} and Si 2p XPS spectra. Pd 3d_{5/2} (**a**) and Si 2p (**b**) XPS spectra of the silicon-nanostructured palladium nanoparticles at a take-off angle of 90° with Ar-ion-sputtering with 3-keV kinetic energy. The nominal etching rate was 0.5 nm/min as SiO₂. The binding energy of Pd(0) in Pd 3d_{5/2} core level is displayed as dotted line at 334.6 eV based on the curve fitting result for the spectrum at the sputtering time of 4 min (Fig. 7).

Methods

General information. See Supplementary Methods.

General procedures. See Supplementary Methods.

Characterization. See Supplementary Figs. 2–26.

X-ray structure determination. See Supplementary Fig. 29 and Supplementary Fig. 30. CIFs are available in Supplementary Data 1–2.

IR Experiments. See Supplementary Fig. 1.

Preparation of a SiNA-stabilized Pd nanoparticle catalyst. A boron doped p-type Si (100) wafer (0.1–100 Ω cm; Φ = 2 inch; 1.5 g; S_{BET} 4 cm²/cm² (Kr)) was immersed in a mixture of conc. 95% H₂SO₄ and 30% H₂O₂ (15 mL: 5 mL, v/v) for 15 min, and then, washed with H₂O and dried with N₂ blow. The washed Si wafer was treated with 5% aqueous HF (10 mL) for 3 min, washed with H₂O, dried with

N₂ blow. One side of Si wafer was masked with a urethane mask sheet (Kokuyo, Co. Ltd). Masked Si wafer was placed into a mixture of 46% HF (15 mL) and AgNO₃ (53.2 mg) in H₂O (47.6 mL), which was slowly stirred for 1 min. The Ag-coated Si wafer was washed with H₂O, and dried with N₂ blow. The urethane mask sheet was peeled off. The Ag-coated Si wafer was placed into a mixture of 46% HF (4.0 mL) and 30% H₂O₂ (0.9 mL) in H₂O (19.0 mL) at 60 °C for 3 min, and Si wafer was washed with H₂O and dried with N₂ blow. The etched Si wafer was immersed

twice in 50% aqueous HNO₃ (30 mL) for 3 min, washed with H₂O, dried with N₂ blow to give the Si nanowire array (SiNA). After SiNA was placed into 5% aqueous HF (10 mL) for 1 min, washed with H₂O, dried with N₂ blow, it was immersed in a mixture of 50 mM aqueous K₂PdCl₄ (4.5 mL) and acetone (1.5 mL) for 5 min. The Si wafer was washed with H₂O and acetone, and dried with N₂ blow to give SiNA-stabilized Pd nanoparticle catalyst (SiNA-Pd). The loading of Pd was determined by ICP-MS.

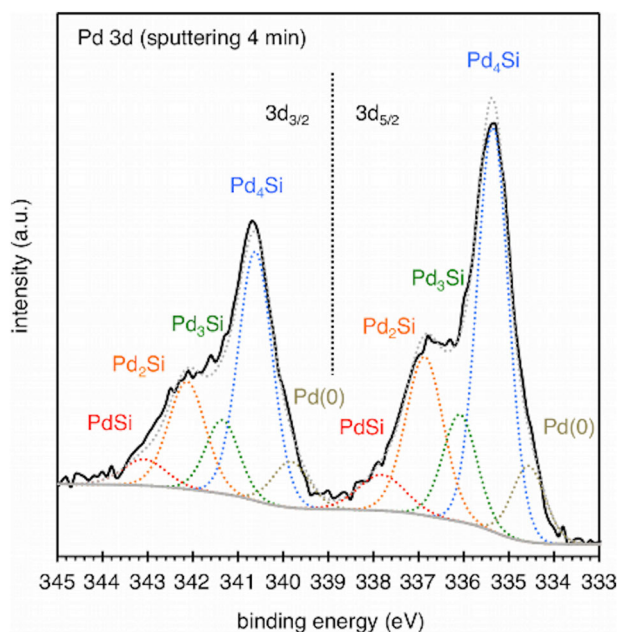


Fig. 7 Pd 3d XPS spectrum of silicon-nanostructured palladium nanoparticles. The black solid line shows the result of the sputtering time of 4 min, and the colored dotted lines do the curve fitting results for Pd(O), Pd₄Si, Pd₃Si, Pd₂Si, and PdSi.

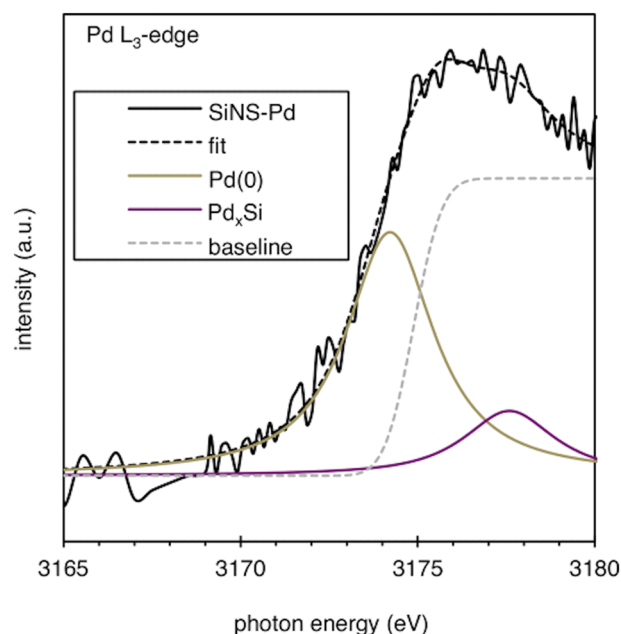
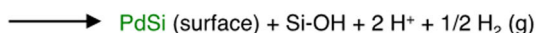
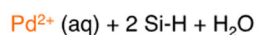
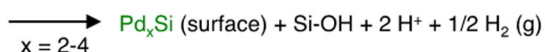
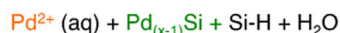


Fig. 8 Curve fitting for the white line in the Pd L3-edge XANES spectrum of silicon-nanostructured palladium nanoparticles. Two pseudo-Voigt functions are applied to Pd(O) and Pd_xSi.

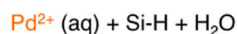
(a) Formation of palladium silicide



(b) Formation of palladium silicide



(c) Reduction of Pd(II) by surface Si-H



(d) Reduction of Pd(II) by Si-Si

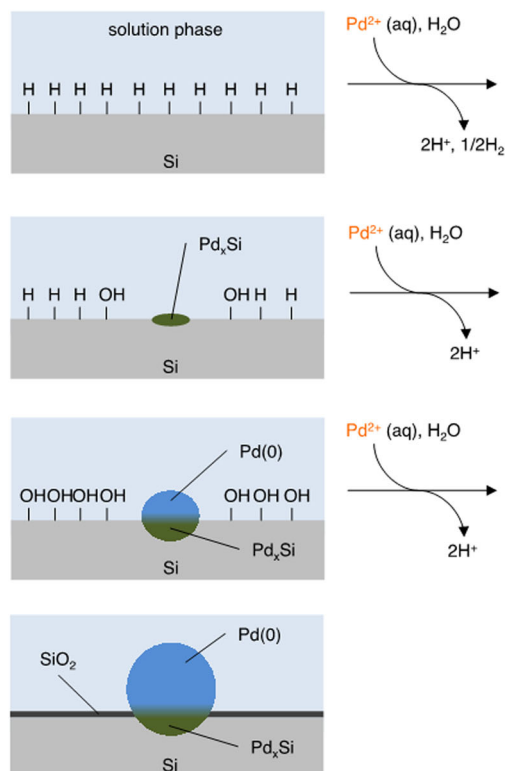
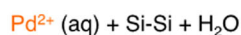


Fig. 9 Plausible mechanism and illustration for immobilization of Pd nanoparticles on silicon surface bridged by palladium silicide layer. a Initial formation of palladium silicide. **b** Consecutive formation of palladium silicide. **c** Reduction of Pd(II) by surface Si-H. **d** Reduction of Pd(II) by Si-Si.

General procedure for the hydrogenation of various substrates. To a 10 mL glass vessel was added SiNA-Pd (0.0025 mmol, 0.05 mol% Pd), each substrate (0.5 mmol), and ethanol (2 mL). The reaction was carried out with H₂ (0.1 MPa, balloon) at 70 °C for 12–24 h under the vortex mixing conditions by a vortex mixer with a temperature controller. After cooling to room temperature, the reaction mixture was analyzed with GC (HP-1) with dodecane or mesitylene as an internal standard to determine the yield.

Catalyst reuse experiments. To a 10 mL glass vessel was added SiNA-Pd (0.0025 mmol, 0.05 mol% Pd), *trans*-stilbene (0.5 mmol, 90 mg), ethanol (2 mL), and dodecane as an internal standard. The reaction was carried out with H₂ (0.1 MPa, balloon) at 70 °C for 24 h under vortex mixer. After cooling to room temperature, the reaction mixture was analyzed with GC (HP-1) to determine the yield. The catalyst was recovered by picking up with a tweezer and washed with EtOAc/acetone/water. After drying with N₂ blow, the catalyst was used for the next reaction.

Data availability

All data supporting the findings of this study are available within the paper as well as the Supplementary Information file, or available from the corresponding authors on reasonable request. The X-ray crystallographic coordinates for structures reported in this Article have been deposited at the Cambridge Crystallographic Data Centre (CCDC), under deposition number CCDC1939498 and CCDC1939526. These data can be obtained free of charge from The Cambridge Crystallographic Data Centre via www.ccdc.cam.ac.uk/data_request/cif.

Received: 16 April 2020; Accepted: 5 June 2020;

Published online: 26 June 2020

References

- Bonrath, W., Medlock, J., Schutz, J., Wustenberg, B. & Netscher, T. in *Hydrogenation* (ed Karam, I.) (InTech, Rijeka, Croatia, 2012).
- Rylander, P. N. *Hydrogenation and Dehydrogenation, Ulmann's Encyclopedia of Industrial Chemistry* (Wiley-VCH, Weinheim, 2005).
- Nishimura, S. *Handbook of Heterogeneous Catalytic Hydrogenation for Organic Synthesis* (Wiley, New York, 2001).
- Rylander, P. N. *Hydrogenation Methods* (Academic Press, New York, 1985).
- Liu, H., Jiang, T., Han, B., Liang, S. & Zhou, Y. Selective phenol hydrogenation to cyclohexanone over a dual supported Pd-lewis acid catalyst. *Science* **326**, 1250–1252 (2009).
- Mastalir, Á., Király, Z. & Berger, F. Comparative study of size-quantized Pd-montmorillonite catalysts in liquid-phase semihydrogenations of alkynes. *Appl. Catal. A* **269**, 161–168 (2004).
- Papp, A., Molnár, Á. & Mastalir, Á. Catalytic investigation of Pd particles supported on MCM-41 for the selective hydrogenations of terminal and internal alkynes. *Appl. Catal. A* **289**, 256–266 (2005).
- Webb, J. D., MacQuarrie, S., McEleney, K. & Crudden, C. M. Mesoporous silica-supported Pd catalysts: an investigation into structure, activity, leaching and heterogeneity. *J. Catal.* **252**, 97–109 (2007).
- Piccolo, L. et al. Tuning the shape of nanoparticles to control their catalytic properties: selective hydrogenation of 1,3-butadiene on Pd/Al₂O₃. *Phys. Chem. Chem. Phys.* **10**, 5504–5506 (2008).
- Domínguez-Domínguez, S., Berenguer-Murcia, Á., Linares-Solano, Á. & Cazorla-Amorós, D. Inorganic materials as supports for palladium nanoparticles: application in the semi-hydrogenation of phenylacetylene. *J. Catal.* **257**, 87–95 (2008).
- Cai, G. et al. Synthesis of a highly stable Pd@CeO₂ catalyst for methane combustion with the synergistic effect of urea and citric acid. *ACS Omega* **3**, 16769–16776 (2018).
- Senfle, T. P., van Duin, A. C. T. & Janik, M. J. Role of site stability in methane activation on Pd₃Ce_{1-x}O₈ surfaces. *ACS Catal.* **5**, 6187–6199 (2015).
- Liu, X. et al. Catalytic partial oxidation of cyclohexane by bimetallic Ag/Pd nanoparticles on magnesium oxide. *Chem. Eur. J.* **23**, 11834–11842 (2017).
- Augustine, R. L. *Catalytic Hydrogenation* (Marcel Dekker, New York, 1965).
- Thomas, J. M., Johnson, B. F. G., Raja, R., Sankar, G. & Midgley, P. A. High-performance nanocatalysts for single-step hydrogenations. *Acc. Chem. Res.* **36**, 20–30 (2003).
- Das, D. D. & Sayari, A. Applications of pore-expanded mesoporous silica 6. novel synthesis of monodispersed supported palladium nanoparticles and their activity for Suzuki reaction. *J. Catal.* **246**, 60–65 (2007).
- Ren, N., Yang, Y.-H., Zhang, Y.-H., Wang, Q.-R. & Tang, Y. Heck coupling in zeolite microcapsular reactor: a test for engaged quasi-homogeneous catalysis. *J. Catal.* **246**, 215–222 (2007).
- Karakanov, E. A., Zolotukhina, A. V., Ivanov, A. O. & Maximov, A. L. Dendrimer-encapsulated Pd nanoparticles, immobilized in silica pores, as catalysts for selective hydrogenation of unsaturated compounds. *Chem. Open* **8**, 358–381 (2019).
- Chen, Z. et al. Pd nanoparticles confined in the porous graphene-like carbon nanosheets for olefin hydrogenation. *Langmuir* **34**, 12809–12814 (2018).
- Budroni, G., Corma, A., Garcia, H. & Primo, A. Pd nanoparticles embedded in sponge-like porous silica as a Suzuki-Miyaura catalyst: similarities and differences with homogeneous catalysts. *J. Catal.* **251**, 345–353 (2007).
- Polshettiwar, V. & Molnár, Á. Silica-supported Pd catalysts for Heck coupling reactions. *Tetrahedron* **63**, 6949–6976 (2007).
- Wisher, A. C., Bronstein, I. & Chechik, V. Thiolated PAMAM dendrimer-coated CdSe/ZnSe nanoparticles as protein transfection agents. *Chem. Commun.* **15**, 1637–1639 (2006).
- Niu, Y., Yeung, L. K. & Crooks, R. M. Size-selective hydrogenation of olefins by dendrimer-encapsulated palladium nanoparticles. *J. Am. Chem. Soc.* **123**, 6840–6846 (2001).
- Gopidas, K. R., Whitesell, J. K. & Fox, M. A. Synthesis, characterization, and catalytic application of a palladium-nanoparticle-cored dendrimer. *Nano Lett.* **3**, 1757–1760 (2003).
- Tang, Z. Core-shell palladium nanoparticle@metal-organic frameworks as multifunctional catalysts for cascade reactions. *J. Am. Chem. Soc.* **136**, 1738–1741 (2014).
- Yamada, Y. M. A. Development of batch and flow immobilized catalytic systems with high catalytic activity and reusability. *Chem. Pharm. Bull.* **65**, 805–821 (2017).
- Hu, H. et al. Self-assembled polymeric pyridine copper catalysts for Huisgen cycloaddition with alkynes and acetylene gas: application in synthesis of tazobactam. *Org. Proc. Res. Dev.* **23**, 493–498 (2019).
- Hudson, R. et al. Poly(meta-phenylene oxides) for the design of a tunable, efficient, and reusable catalytic platform. *Chem. Commun.* **54**, 2878–2881 (2018).
- Yamada, Y. M. A., Sarkar, S. M. & Uozumi, Y. Amphiphilic self-assembled polymeric copper catalyst to parts per million levels: click chemistry. *J. Am. Chem. Soc.* **134**, 9285–9290 (2012).
- Yamada, Y. M. A., Sarkar, S. M. & Uozumi, Y. Self-assembled poly(imidazole-palladium): highly active, reusable catalyst at parts per million to parts per billion levels. *J. Am. Chem. Soc.* **134**, 3190–3198 (2012).
- Sarkar, S. M., Uozumi, Y. & Yamada, Y. M. A. A highly active and reusable self-assembled poly(imidazole/palladium) catalyst: allylic arylation/alkenylation. *Angew. Chem. Int. Ed.* **50**, 9437–9441 (2011).
- Chng, L. L., Erathodiyil, N. & Ying, J. Y. Nanostructure catalysts for organic transformations. *Acc. Chem. Res.* **46**, 1825–1837 (2013).
- Yamada, Y. M. A. et al. A palladium-nanoparticle and silicon-nanowire-array hybrid: a platform for catalytic heterogeneous reactions. *Angew. Chem. Int. Ed.* **53**, 127–131 (2014).
- Baek, H. et al. Production of bio hydrofined diesel, jet fuel, and carbon monoxide from fatty acids using a silicon nanowire array-supported rhodium nanoparticle catalyst under microwave conditions. *ACS Catal.* **10**, 2148–2156 (2020). For Rh nanoparticles on SiNA, see.
- Casiello, M. et al. Catalytic activity of silicon nanowires decorated with gold and copper nanoparticles deposited by pulsed laser ablation. *Nanomaterials* **8**, 78–95 (2018).
- Sun, X.-H. et al. Reductive self-assembling of Pd and Rh nanoparticles on silicon nanowire templates. *Chem. Mater.* **16**, 1143–1152 (2004).
- Schmidt, V., Wittemann, J. V. & Gösele, U. Growth, thermodynamics, and electrical properties of silicon nanowires. *Chem. Rev.* **110**, 361–388 (2010).
- Niwano, M., Miura, T., Kimura, Y., Tajima, R. & Miyamoto, N. Real-time, in situ infrared study of etching of Si (100) and (111) surfaces in dilute hydrofluoric acid solution. *J. Appl. Phys.* **79**, 3708–3713 (1996).
- Niwano, M., Takeda, Y., Ishibashi, Y., Kurita, K. & Miyamoto, N. Morphology of hydrofluoric acid and ammonium fluoride-treated silicon surfaces studied by surface infrared spectroscopy. *J. Appl. Phys.* **71**, 5646–5649 (1992).
- Trucks, G. W., Raghavachari, K., Higashi, G. S. & Chabal, Y. J. Mechanism of HF etching of silicon surfaces: a theoretical understanding of hydrogen passivation. *Phys. Rev. Lett.* **65**, 504–507 (1990).
- Zhang, M.-L. et al. Preparation of large-area uniform silicon nanowires arrays through metal-assisted chemical etching. *J. Phys. Chem. C* **112**, 4444–4450 (2008).
- Yang, S. et al. Nanoscale magnetic stirring bars for heterogeneous catalysis in microscopic systems. *Angew. Chem. Int. Ed.* **54**, 2661–2664 (2015).
- Wei, F. et al. In situ facile loading of noble metal nanoparticles on polydopamine nanospheres via galvanic replacement reaction for multifunctional catalysis. *Sci. China Chem.* **60**, 1236–1242 (2017).
- Besson, M., Gallezot, P. & Pinel, C. Conversion of biomass into chemicals over metal catalysts. *Chem. Rev.* **114**, 1827–1870 (2014).
- Pews-Davtyan, A. et al. Biomolecule-derived supported cobalt nanoparticles for hydrogenation of industrial olefins, natural oils and more in water. *Green. Chem.* **21**, 5104–5112 (2019).

46. McArdle, S., Girish, S., Leahy, J. J. & Curtin, T. Selective hydrogenation of sunflower oil over noble metal catalysts. *J. Mol. Catal. A: Chem.* **351**, 179–187 (2011).
47. Maki-Arvela, P. catalytic hydrogenation of linoleic acid to stearic acid over different Pd- and Ru-supported catalysts. *Appl. Catal., A: Gen.* **345**, 201–212 (2008).
48. Roach, C. et al. Comparison of cis and trans fatty acid containing phosphatidylcholines on membrane properties. *Biochemistry* **43**, 6344–6351 (2004).
49. Emken, E. A. Nutrition and biochemistry of trans and positional fatty acid isomers in hydrogenated oil. *Rev. Nutr.* **4**, 339–376 (1984).
50. Mozaffarian, D. et al. Trans fatty acids and cardiovascular disease. *N. Engl. J. Med.* **354**, 1601–1613 (2006).
51. Hofmann, S. Compositional depth profiling by sputtering. *Prog. Surf. Sci.* **36**, 35–87 (1991).
52. Chen, L.-Y., Hunter, G. W., Neudeck, P. G. & Knight, D. X-ray photoelectron spectroscopy study of the heating effects on Pd/6H-SiC Schottky structure. *J. Vac. Sci. Technol., A* **16**, 2890–2895 (1998).
53. Lidiya, L. S., Stadnichenko, A. I., Koscheev, S. V., Zaikovskii, V. I. & Boronin, A. I. Highly oxidized palladium nanoparticles comprising Pd⁴⁺ Species: spectroscopic and structural aspects, thermal stability, and reactivity. *J. Phys. Chem. C* **116**, 19342–19348 (2012).
54. Shaplugin, I. S., Aparnikov, G. L. & Lazarev, V. B. Preparation of palladium dioxide at high pressure. *Zh. Neorg. Khim.* **23**, 884–887 (1978).
55. Kibis, L. S., Titkov, A. I., Stadnichenko, A. I., Koscheev, S. V. & Boronin, A. I. X-ray photoelectron spectroscopy study of Pd oxidation by RF discharge in oxygen. *Appl. Surf. Sci.* **255**, 9248–9254 (2009).
56. Grunthaner, P. J., Grunthaner, F. J., Madhukar, A. & Mayer, J. W. metal/silicon interface formation: the Ni/Si and Pd/Si systems. *J. Vac. Sci. Technol.* **19**, 649–656 (1981).
57. Atzrodt, V., Wirth, T. H. & Lange, H. Investigation of NiSi and Pd₃Si thin films by AES and XPS. *Phys. Status Solidi (a)* **62**, 531–537 (1980).
58. Wagner, C. D. & Taylor, J. A. Generation of XPS auger lines by bremsstrahlung. *J. Electron Spectrosc. Relat. Phenom.* **20**, 83–93 (1980).
59. Chen, J. G. NEXAFS investigations of transition metal oxides, nitrides, carbides, sulfides and other interstitial compounds. *Surf. Sci. Rep.* **30**, 1–152 (1997).
60. Mason, M. G. Electronic structure of supported small metal clusters. *Phys. Rev. B* **27**, 748–762 (1983).
61. Kubota, T., Kitajima, Y., Asakura, K. & Iwasawa, Y. Pd L₃-edge XANES spectra of supported Pd particles induced by the adsorption and the absorption of hydrogen. *Bull. Chem. Soc. Jpn.* **72**, 673–681 (1999).

Acknowledgements

The authors would like to thank Dr. Daisuke Hashizume (Materials Characterization Support Team, CEMS, RIKEN, Japan) for X-ray crystallography, Dr. Tetsuo Honma (JASRI) for hard X-ray XAFS experiment, and Ms. Aya Ohno (our team) for ICP-MS

analysis. We are also very grateful to Prof. Toshiaki Ohta and Dr. Keisuke Yamanaka (SR Center, Ritsumeikan University) for soft X-ray XAFS experiments. Mass spectral data were acquired at the mass spectrometry facility run by Molecular Structure Characterization Unit (RIKEN CSRS, Wako). We gratefully acknowledge financial support from the JST ACT-C (#JPMJCR12ZC), the JST ACCEL (#JPMJAC1401), the JSPS (#24550126, #20655035, and #15K05510), AMED (#19ak0101115h), the Takeda Science Foundation, the Naito Foundation, and RIKEN.

Author contributions

Y.M.A.Y. and Y.U. conceived the work and designed the experiments. H.B. carried out the catalytic reactions. A.N. conducted the XPS measurements. T.S. prepared the silicon Pd devices for XPS measurements and the spectroscopic measurements. All the authors contributed to intellectual insights of this work. Y.M.A.Y., H.B., and T.S. wrote the paper, and all authors edited the paper.

Competing interests

The authors declare no competing interests.

Additional information

Supplementary information is available for this paper at <https://doi.org/10.1038/s42004-020-0332-z>.

Correspondence and requests for materials should be addressed to Y.M.A.Y.

Reprints and permission information is available at <http://www.nature.com/reprints>

Publisher's note Springer Nature remains neutral with regard to jurisdictional claims in published maps and institutional affiliations.



Open Access This article is licensed under a Creative Commons Attribution 4.0 International License, which permits use, sharing, adaptation, distribution and reproduction in any medium or format, as long as you give appropriate credit to the original author(s) and the source, provide a link to the Creative Commons license, and indicate if changes were made. The images or other third party material in this article are included in the article's Creative Commons license, unless indicated otherwise in a credit line to the material. If material is not included in the article's Creative Commons license and your intended use is not permitted by statutory regulation or exceeds the permitted use, you will need to obtain permission directly from the copyright holder. To view a copy of this license, visit <http://creativecommons.org/licenses/by/4.0/>.

© The Author(s) 2020